Theoretical Modeling Coupled with Experimental Study on the Preparation and Characterization Comparison of Fluorinated Copolymers: Effect of Chain Structure on Copolymer Properties

Yin-Ning Zhou and Zheng-Hong Luo
Dept. of Chemical Engineering, Shanghai Jiao Tong University, Shanghai 200240, P. R. China

Dept. of Chemical and Biochemical Engineering, Xiamen University, Xiamen 361005, P. R. China

Jian-Hua Chen
Dept. of Chemistry and Environmental Science, Zhangzhou Normal University, Zhangzhou 363000, P.R. China

DOI 10.1002/aic.14057
Published online March 4, 2013 in Wiley Online Library (wileyonlinelibrary.com)

Theoretical modeling coupled with an experimental study is presented for the preparation and characterization comparison of the amphiphilic copolymers of 2, 2, 3, 3, 4, 4, 4-heptafluorobutyl methacrylate (HFBMA) and 2-hydroxyethyl methacrylate (HEMA) to achieve a multiscale generalization of the polymeric system. A series of amphiphilic copolymers having different chain structures with HFBMA as the hydrophobic component and HEMA as the hydrophilic component was first synthesized through atom transfer radical copolymerization (ATRcoP) or model-based semibatch ATRcoP. Theoretical modeling is used to optimize the macromolecular structure and experimental approaches that are used to prepare copolymers of HFBMA and HEMA with some tailor-made polymer properties. Furthermore, a systematic comparison of major properties (i.e., thermal, micellization, and surface properties) of these fluorinated copolymers (i.e., random, block, linear gradient, and inverse linear gradient copolymers) was carried out. The results show that these fluorinated copolymers with different chain structures have dissimilar properties. The results also demonstrate that the approach of coupling theoretical modeling with an experimental study can be used to guide a multiscale generalization of the polymeric system for practical application. © 2013 American Institute of Chemical Engineers *AIChE J*, 59: 3019–3033, 2013

Keywords: atom transfer radical polymerization, theoretical modeling coupled with experimental approachest, fluorinated copolymers, thermal property, micellization, surface property

Introduction

Fluorinated (co)polymers have attracted much attention because of their excellent properties such as high hydrophobicity, thermal stability, chemical stability, permeability, and biocompatibility, and so forth.[1–10] On the other hand, poly(2-hydroxyethyl methacrylate) (PHEMA) shows excellent biocompatible and water-swellable properties, and so forth.[11–14] PHEMA oligomers are water-soluble,[15–19] but high-molecular-weight PHEMA homopolymer is generally regarded as being only water-swellable instead of water-soluble.[14,16,20,21] With the fluorinated polymer being hydrophobic and PHEMA polymer being hydrophilic, the copolymers of HEMA and fluorinated comonomers, such as 2,2,3,3,4,4,4-heptafluorobutyl methacrylate (HFBMA), have the combined valuable properties of both homopolymers, including their amphiphilicity. Proper tuning of copolymer composition and composition distribution is expected to render a range of copolymers with tailor-designed properties.[8,16]

Generally, copolymers having a given cumulative composition can be classified into different types, including random, block, and gradient copolymers, according to their composition distribution. Typically, random copolymers possess constant average composition along the chain, and block copolymers show an abrupt step change in composition at the block joint location.[22] Thus, random copolymers have more advantages in compatibility with different components block copolymers consisting of two or more chemically dissimilar thermodynamically incompatible blocks tend to form self-assembled ordered structures with periodicity or compositional heterogeneity on a nanometer length scale. On the other hand, gradient copolymers show a gradual continuous change in composition from one end of the chain to the other.[23] Thus, they constitute a relatively new class of polymers with a molecular structure spanning between those of random and block copolymers with interesting properties (e.g., extremely broad glass transition temperature range). Arising from their unique structures and properties, gradient copolymers find some featured applications including additives in cosmetics, compatibilizers in polymer blends, and damping materials.

Additional Supporting Information may be found in the online version of this article.

Correspondence concerning this article should be addressed to Z. H. Luo at luozh@xmu.edu.cn.

As has been confirmed through both theoretical and experimental approaches, copolymer composition distribution (CCD) is an important microstructural parameter affecting physical and functional properties of polymer materials.[24–30] For instance, Torkelson and coworkers[25–27] have shown the composition distribution can significantly influence the breadth of glass transition temperatures (ΔT_gs) in random, block, and gradient copolymers. A full understanding of the relationship between chain structure and polymer properties is, thus, critical to achieve a multiscale generalization of a polymeric system from polymer design to its practical application. With specific regard to the copolymers of HFBMA and HEMA as a model system, establishing the relationship between chain structure and polymer properties is necessary for the tailored design and applications of these valuable polymeric materials.

The recent advent of controlled/living radical polymerization (CLRP) techniques has made it possible to design the fluorinated copolymer chain structure with the expected property.[31] Some most notable CLRP mechanisms include that nitroxide-mediated polymerization (NMP),[32,33] atom transfer radical polymerization (ATRP),[34–37] reversible addition fragmentation chain transfer (RAFT) polymerization,[38,39] and single-electron transfer and single-electron transfer degenerative chain transfer CLRP,[40,41] and so forth. Generally, introducing a comonomer in CLRP offers the possibility of preparing tailor-made copolymers with certain desired properties. However, in a batch process, composition drift is very common due to the difference in the reactivity ratio of the monomers. To control copolymer composition, a semibatch operation is commonly used. The copolymers with uniform composition or linear gradient composition can be successfully designed and controlled through optimizing monomer feeding to a semibatch reactor.[42–47] For instance, Wang and Broadbelt[42,43] introduced a computational tool based on kinetic Monte Carlo simulations for NMP, which can generate recipes for synthesis of copolymers of predesigned monomer sequences, but they did not predict any materials properties. Luo and coworkers[44–47] developed kinetic models for semibatch RAFT copolymerization and atom transfer radical copolymerization (ATRcoP). Their work has demonstrated the feasibility of the control of CCD using a semibatch feeding policy. However, the relationship between CCD/chain structure and polymer properties was not investigated in their work.[42–47] Furthermore, the above polymerization systems did not involve the copolymerization of HFBMA and HEMA.

In this work, we attempt to develop a combinatory strategy which couples both theoretical modeling and experimental investigations for optimizing the macromolecular structure of copolymers of HFBMA and HEMA to achieve some targeted polymer properties. Previous studies have noted that thermal stability,[8] surface property,[48–50] and self-assembly behavior[51–55] in dilute solution as the most outstanding properties of the fluorinated copolymers. Therefore, thermal, micellization, and surface properties are selected herein as the target polymer properties.

We first focus on using theory models to design and control synthesis of new and well-defined copolymers of HEMA and HFBMA via ATRcoP, sequential ATRP in batch and model-based semibatch ATRcoP through controlling the polymerization conditions (i.e., time, amount of initiator and monomers, feeding rate). Meanwhile, a systematic study is put forward to compare the thermal, micellization, and surface properties of these fluorinated copolymers with different chain structures to establish the relationships between the chain structure and polymer properties. Especially, one can benefit from an idea of whole contribution shown in Scheme 1 that correlates the chain structure with the desired properties, for example, when one needs a fluorinated polymeric material with broader glass transition region and relatively strong hydrophobic characteristics, the linear gradient copolymer would be the best choice, whereas if a broader glass transition region is the only requirement, the inverse linear gradient copolymer can be chosen.

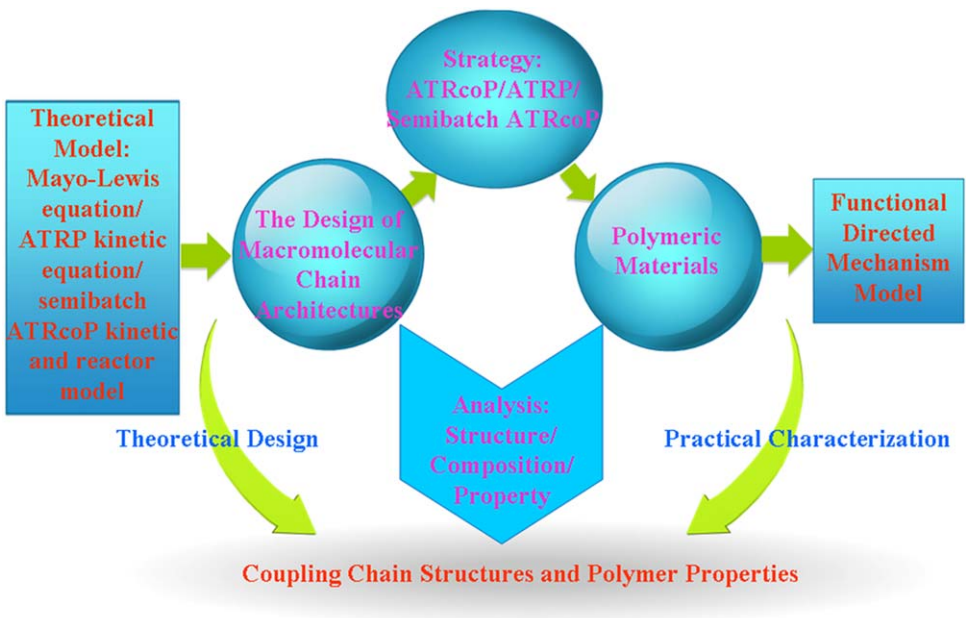

Scheme 1. Schematic design idea of the whole contribution.

[Color figure can be viewed in the online issue, which is available at wileyonlinelibrary.com]

Theory

CLRP has become the most powerful tool for preparing copolymers with tailored polymer chain structures, such as gradient, random, and block. For a copolymerization system with similar reactivity ratio of comonomers, well-defined copolymers can be synthesized via ATRP based on theoretical modeling. The theoretical modeling illustrated in Scheme 1 includes three aspects:

1. The classical Mayo–Lewis model is applied to determinate the composition of a random copolymer in batch copolymerization by the total conversion (C), the reactivity ratios (r_1 and r_2), and the initial fraction for both monomers in the feed solution (f_1 and f_2). The main equations are as follows[56]

$$F_1 = \frac{r_1 f_1^2 + f_1 f_2}{r_1 f_1^2 + f_1 f_2 + r_2 f_2^2}, \tag{1}$$

$$\bar{F}_1 = \frac{f_0^1 - (1-C) f_1}{C}, \tag{2}$$

where F_1 and $\bar{F}_1$ represent the instantaneous mole fraction and average composition of monomer 1 (M_1) in the copolymer, respectively, The subscript of zero indicates initial quantity. A useful method for analyzing copolymer composition as a function of conversion was suggested by Skeist in 1946.[57] A material balance for M_1 requires that the mole number of M_1 copolymerized equals to the difference of mole number of M_1 in the feed before and after reaction, can be given by

$$Mf_1 - (M - dM)(f_1 - df_1) = F_1 dM, \tag{3}$$

where M is the total monomer mole number. Equation 3 can be rearranged when neglecting the term of $dMdf_1$ (because it is very small). Thus, the following equation via integrating is obtained

$$\int_{M_0}^{M} \frac{dM}{M} = \ln \frac{M}{M_0} = \int_{f_1^0}^{f_1} \frac{df_1}{F_1 - f_1}. \tag{4}$$

Furthermore, Meyer integrated Eq. 4 integrated to an useful closed form using Eq. 1 in 1965,[58] which relates the degree of conversion to changes in the comonomer feed composition

$$C = 1 - \frac{M}{M_0} = 1 - \left[\frac{f_1}{f_1^0}\right]^{\alpha} \left[\frac{f_2}{f_2^0}\right]^{\beta} \left[\frac{f_1^0 - \delta}{f_1 - \delta}\right]^{\gamma}, \tag{5}$$

where, $\alpha = r_2/(1-r_2), \beta = r_1/(1-r_1), \gamma = (1-r_1 r_2)/[(1-r_1)(1-r_2)]$, and $\delta = (1-r_2)/(2-r_1-r_2)$.

For a living copolymerization, the average composition of the polymer chain is a function of chain length and can be easily described by the above integrated copolymerization composition equation.[59]

2. The kinetic model of living polymerization, which is characterized by linearity of the first-order kinetics, can be used to optimize the specific composition of a block copolymer in sequential batch polymerization by reaction time and amount of initiator. The theoretical molecular weight ($M_{n,theo}$) increases reciprocally with the initial concentration of initiator ($[I]$) in a living polymerization (Eq. 6).[34]

$$M_{n,theo} = M_{n,monomer} \times \frac{[M]_0}{[I]_0} \times C. \tag{6}$$

The kinetic equation of ATRP has been derived by Matyjaszewski and Xia[34] based on the assumption that the contribution of termination becomes insignificant due to the persistent radical effect and using a fast equilibrium approximation, which is necessary for the observed low polydispersities as follows

$$-\frac{d[\mathrm{M}]}{dt} = k_p[\mathrm{P}\cdot][\mathrm{M}] = k_p K_{ATRP} [I]_0 \frac{[Cu(\mathrm{I})\mathrm{L}]}{[Cu(\mathrm{II})\mathrm{L}]} [\mathrm{M}] = k_p^{app} [\mathrm{M}], \tag{7}$$

where k_p, K_{ATRP}, and $k_p^{app} = k_p K_{ATRP} [I]_0 \frac{[Cu(\mathrm{I})\mathrm{L}]}{[Cu(\mathrm{II})\mathrm{L}]}$ represent the chain propagation rate constant, equilibrium constant, and the chain propagation apparent rate constant, respectively. $[Cu(\mathrm{I})L]$ and $[Cu(\mathrm{II})L]$ stand for the concentration of activator and deactivator, respectively. Therefore, the logarithmic monomer concentration gradually increases with time and can be described via Eq. 8, which is obtained by integrating Eq. 7.

$$\ln\left(\frac{[\mathrm{M}]_0}{[\mathrm{M}]}\right) = \ln\left(\frac{1}{1-C}\right) = k_p^{app} \mathrm{t}. \tag{8}$$

3. In our previous work,[30] we have developed a detailed kinetic model for the semibatch ATRcoP for synthesis of gradient copolymers via controlling the polymerization conditions (i.e., time, feeding rate, amount of initiator, and monomers). The elementary reactions involved in the model, kinetic equations and definitions of moments, diffusion-controlled pseudokinetic rate constants, and the semibatch reactor model are briefly summarized in Supporting Information, Tables S1–S4, respectively. A complete set of moment equations has been derived as summarized in Supporting Information, Table S5. Therefore, one can readily simulate the polymerization kinetics when given the initial conditions (concentration of monomer, monomer feeding rate, etc.) and the major parameters (listed in Supporting Information, Tables S6 and S7). On the other hand, the model can be applied to optimize the feeding rate to reach the desired copolymer composition, *Conv*. and *Mn*.

Experimental

Materials

HFBMA (98%) and ethyl 2-bromoisobutyrate (Eib-Br, 98%) were obtained from A Better Choice for Research Chemicals GmbH & Co. KG. (ABCR). HFBMA was rinsed with 5-wt % aqueous NaOH solution to remove the inhibitor. HEMA (95%) and tetrabutylammonium fluoride [TBAF, 1 M in tetrahydrofuran (THF)] were obtained from TCI (Shanghai) Development Co. HEMA was purified by washing an aqueous solution of monomer with hexane to remove ethylene glycol dimethacrylate, salting the monomer out of the aqueous phase by addition of NaCl, drying over $MgSO_4$, and distilling under reduced pressure. 4,4'-dinonyl-2,2'-bipyridyl (dNbpy, Nanjing Chemzam Pharmtech, 99%) was recrystallized three times from ethanol. CuBr [Sinopharm Chemical Reagent Co. (SCRC), 99%] was purified by washing with acetic acid and methanol alternatively three times, and dried under vacuum at 45°C for 24 h. Potassium fluoride (KF, 99%, SCRC) was used as received. All other reagents

and solvents were obtained from SCRC and used without further purification.

Synthesis of HEMA-2-(trimethylsilyl) ethyl methacrylate

Due to its poor solubility in low-polarity solvents, HEMA is often polymerized in its protected form, 2-(trimethylsilyl) ethyl methacrylate (HEMA-TMS). The detailed synthesis procedure for HEMA-TMS can be found in Ref. 60.

Synthesis of P(HEMA-TMS-HFBMA) random, diblock, and gradient copolymers

Random copolymers were synthesized using batch ATRP with Eib-Br as initiator. The comonomers, solvent (toluene), and catalyst system (CuBr, $CuBr_2$, dNbpy) were combined in a dried round-bottom flask, and the mixture was degassed three times by freeze/pump/thaw cycles. After that, the initiator Eib-Br was added under N_2.

Diblock copolymers were synthesized through sequential batch ATRP. The PHEMA-TMS macroinitiator was first synthesized in toluene with Eib-Br as initiator. The macroinitiator was then used to prepare the diblock copolymers using HFBMA as the second monomer.

Gradient copolymers were synthesized through semibatch ATRP which is described in Scheme 2. A typical procedure can be described as follows: toluene, catalyst system, and HFBMA or HEMA-TMS were first added to a dried round-bottom flask; in a second reaction flask, catalyst system and HEMA-TMS or HFBMA were added and degassed by three freeze/pump/thaw cycles. After that, the initiator Eib-Br was added. The secondary reaction mixture was transferred into an airtight syringe and assembled to a syringe pump. Synchronously, the continuous addition of the secondary reaction mixture to the primary one was started at an optimized feeding rate, which is designed to obtain the expected monomer conversion.

The reactions were carried out in a preheated oil bath at 80°C and stopped after 7 h by cooling the flask to room-temperature and exposing the reaction mixture to air. Samples (about 0.1–0.2 mL) were taken for determining the cumulative composition by nuclear magnetic resonance (^{1}H NMR). The resulting polymers were obtained by removing the catalyst, evaporating the solvent and residual monomer, precipitating in petroleum ether (60–90°C), and finally drying under vacuum. Monomer conversion was measured by gravimetry. Recipes for all the experimental studies are listed in Table 1 (Expt. 1 and 2 are used to synthesize the polymers with linear gradient and inverse linear gradient composition, respectively; Expt. 3 and 4 are for synthesizing the random and biblock copolymers, respectively).

Preparation of P(HEMA-HFBMA) random, diblock, and gradient copolymers

HFBMA/HEMA-TMS copolymer (1 g) synthesized above was dissolved in 20 mL of dry THF. KF (30 mg, 0.5 mmol) and TBAF (50 μL, 0.05 mmol) were added to the polymer solution and stirred for 24 h at 30°C. A part of the solvent was evaporated under reduced pressure, and the polymer was precipitated in water. After filtration, the polymer was dried under vacuum for 24 h, and the copolymer of HFBMA/HEMA was obtained.

Preparation of the copolymers aggregates

The procedure of preparation of micellar solutions is described as follows: copolymers were first dissolved in THF, followed by the dropwise addition of a selective solvent (H_2O) under vigorous stirring to reach a predetermined amount (THF/H_2O = 4/1 vol.). Then, the bottle was sealed and left for 72 h before measurement at room-temperature. The concentration of polymer solutions was fixed at 1 mg/mL.

Preparation of the copolymers membranes

The resulting copolymers were dissolved in THF at a certain concentration (3 wt %). The polymer solution was directly cast and coated onto a clean glass slide or a clean silicon wafer for different test requirements, and then dried naturally in an ambient environment for 24 h using a polymer solution evaporation method.

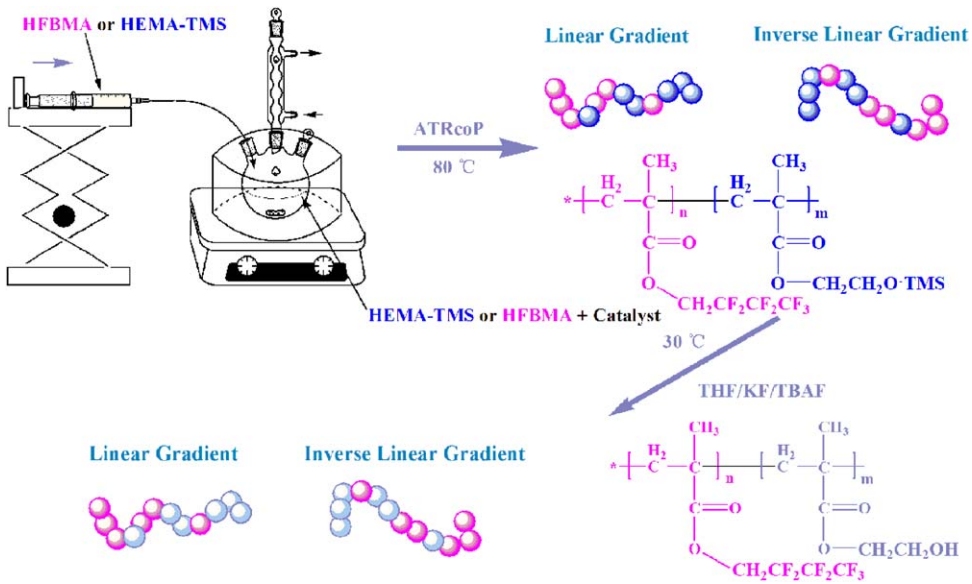

Scheme 2. Experimental apparatus for the semibatch ATRcoP.

[Color figure can be viewed in the online issue, which is available at wileyonlinelibrary.com]

Table 1. Recipes for All the Experimental Studies

Expt.		HFBMA (mmol)(mL)	HEMA-TMS (mmol)(mL)	Initiator (mmol)	CuBr (mmol)	$CuBr_2$ (mmol)	dNbpy (mmol)	Solvent (mL)	V_f (mL/h)
1	r. f.	10(2.0)	–	0.2	0.2	0.01	0.4	3	–
	a. s.	–	10(2.1)		0.2	0.01	0.4	3	0.7286
2	r. f.		10(2.1)	0.2	0.2	0.01	0.4	3	–
	a. s.	10(2.0)	–		0.2	0.01	0.4	3	0.7143
3	r. f.	7(1.4)	13(2.7)	0.2	0.4	0.02	0.8	6	–
4	r. f.	10(2.0)	–	0.2	0.2	0.01	0.4	6	–

r. f. = reactive flask; a. s. = airtight syringe.

Measurements

Nuclear Magnetic Resonance. The copolymer compositions were determined by ^1H NMR spectroscopy (Bruker AV400 MHz) in dimethyl sulfoxide-d_6.

Fourier-Transform Infrared. Fourier-transform infrared (FTIR) spectra were recorded using KBr pellets on a Nicolet Avatar 360-FTIR spectrophotometer.

Gel Permeation Chromatography. The molecular weight (M_n) and molecular weight distribution [M_w/M_n, polydispersity index (PDI)] of the polymer were determined at 40°C by gel permeation chromatography (GPC) equipped with a waters 1515 isocratic HPLC pump, three Styragel columns (Waters HT4, HT5E, and HT6), and a waters 2414-refractive index detector (set at 30°C). THF was used as the eluent at a flow rate of 1.0 mL/min. A series of poly(methyl methacrylate) narrow standards were used to generate a universal calibration curve.

Differential Scanning Calorimeter. The thermal analysis of the P(HEMA-HFBMA) copolymers was carried out using a differential scanning calorimeter (Netzsch DSC 204). Cooling was accomplished by a liquid nitrogen cooling accessory. Around 10 mg of sample was loaded into an aluminum pan with an empty pan serving as a reference. Dry nitrogen was purged into the DSC cell at a flow rate of 50 mL/min. The samples were first heated at a rate of 10°C/min to 150°C and held at 150°C for 5 min to eliminate thermal history. The samples were then cooled at a rate of −40°C/min to 0°C before being reheated to 150°C at a rate of 10°C/min. All data associated with the glass transition measurements were obtained from the second heating scan.

Transmission Electron Microscopy. The morphology of the P(HEMA-HFBMA) copolymers was observed by transmission electron microscopy (TEM). A drop of polymer solution was placed onto a copper grid coated with carbon, and the grid was then left to dry in a desiccator for 72 h to eliminate trace solvent. The sample was used without any staining procedure. A transmission electron microscope (JEM-2100) was used at an accelerating voltage of 200 kV.

Dynamic Light Scattering. Dynamic light scattering (DLS) experiments were performed using an Malvern light scattering instrument equipped with a 400-mW argon ion laser with wavelength of 532 nm, and scattering angle was 90°. Temperatures were controlled by a Haake C35 thermostat, providing an accuracy of 0.1 K.

Static Water Contact Angle. The static water contact angles (SWCAs) were recorded on a Contact Angle Measuring Instrument (KRUSS, DSA30) by the sessile drop method with a microsyringe at room-temperature on a 75 × 15 × 1 mm^3 glass slice covered with the resulting polymer membranes. The injection volume of liquid is 5 μL. For

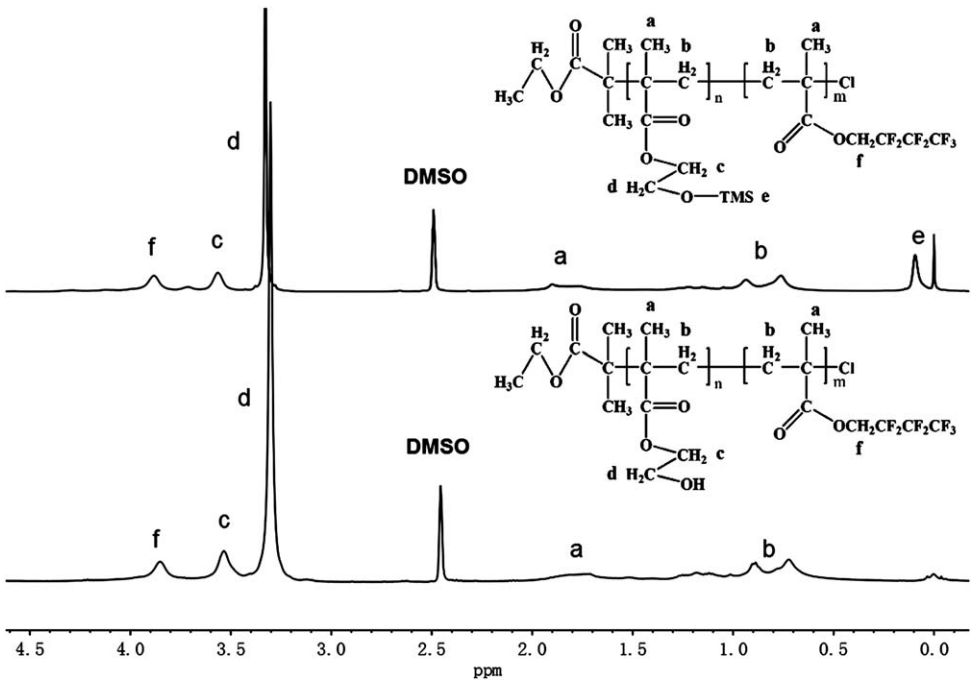

Figure 1. ^1H NMR spectrum of the HFBMA/HEMA and HFBMA/HEMA-TMS linear gradient copolymers.

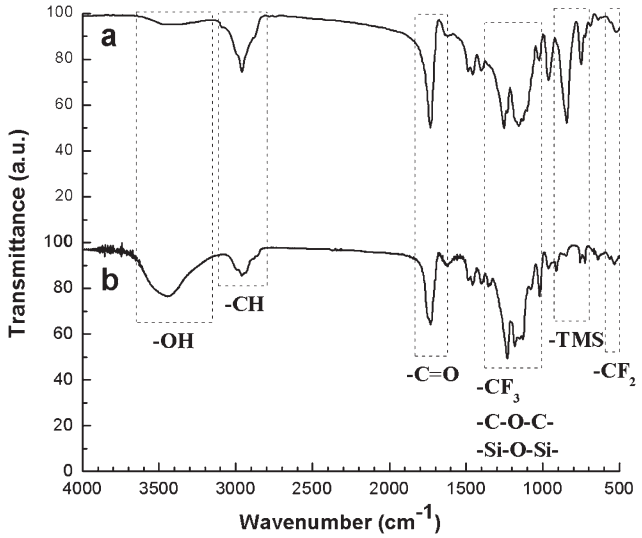

Figure 2. FTIR spectrum of the HFBMA/HEMA-TMS (a) and HFBMA/HEMA (b) linear gradient copolymers.

each angle reported, at least five readings from different locations were averaged.

X-Ray Photoelectron Spectroscopy. X-ray photoelectron spectroscopy (XPS) spectra were recorded to determine the surface composition of the resulting polymer films using a PHI quantum 2000 scanning ESCA microprobe (physical electronic, USA), equipped with an Al Kα1, 2 monochromatic source of 1486.60 eV. The samples were measured on a silicon slice.

Results and Discussion

Synthesis of well-defined amphiphilic fluorinated copolymers

In this work, according to the guidance of theory models, batch ATRcoP and sequential ATRP were chosen to prepare the fluorinated random and diblock copolymers with well-defined microstructure, targeted M_n with similar fluorine content, respectively. However, gradient copolymers with linear and inverse linear gradient composition were synthesized via model-based semibatch ATRcoP. The comprehensive mathematical model was used to optimize the feeding rate to obtain the targeted monomer conversion and precise-gradient chain structure.[30]

The overall ratio of incorporated monomers in resulting copolymers (HFBMA/HEMA-TMS) was determined using ^{1}H NMR measurements (Figure 1, taking linear gradient copolymer, for example). This was done by comparing the peak area ratio of characteristic signals for HFBMA (4.4 ppm 2H, —$OCH_2(CF_2)_2CF_3$) and PHEMA-TMS (3.94 ppm, 2H, —CH_2—OCO— and 3.62 ppm, 2H, —CH_2—O—$Si(CH_3)_3$; 0.05–0.16 ppm, 9H, —$Si(CH_3)_3$). The structure was also characterized by FTIR (Figure 2a): (2800–3000 cm^{-1} (the vibration of —CH), 1753 cm^{-1} (the vibration of —C═O), 1232–1128 cm^{-1}, (the antisymmetric and symmetric stretching vibrations of the —CF_3), 536 cm^{-1} (the combination of the cocking and wagging vibrations of the —CF_2), 1050–1250 cm^{-1}(the stretching vibrations of —C—O—C— and -Si—O—Si-), 700–850 cm^{-1}(the vibration of —TMS)).

In addition, the ^{1}H NMR (Figure 1) and FTIR (Figure 2b) results indicate that the TMS group on the copolymers was fully removed (absence of —O—TMS resonance δ=0.05−0.16 ppm (9H, —$Si(CH_3)_3$) and 700–850 cm^{-1} for the vibration of —TMS, presence of 3200–3600 cm^{-1} for the vibration of —OH). Consequently, one can know that the copolymers of HFBMA/HEMA were obtained.

For the gradient copolymers with a symmetric composition along the chain, two approaches can be used to synthesize them with different direction of chain growth. For example, if someone charges all HFBMA into the reactor and feeds the HEMA-TMS with a metering pump (Normal Mode), a linear gradient copolymer will be synthesized (Expt. 1). On the contrary, exchanging the monomer feeding sequence (Inverse Mode), we can synthesize an inverse linear gradient copolymer (Expt. 2). To monitor monomer sequence distribution in the products during the synthesis of gradient copolymers, reaction aliquots were taken to verify the change in cumulative composition (F_{cum}) of feeding monomer (M_2) as a function of chain length. It should be pointed out that the instantaneous

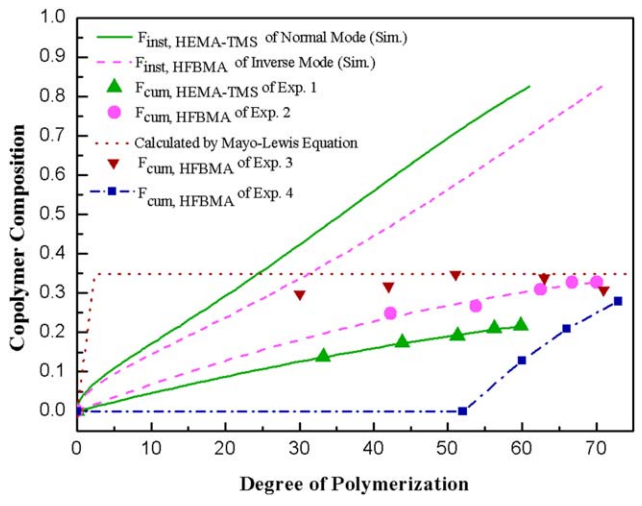

Figure 3. Copolymer composition as a function of the degree of polymerization (Lines are predicted by theoretical modeling and Symbols represent experimental data measured by ^{1}H NMR).

[Color figure can be viewed in the online issue, which is available at wileyonlinelibrary.com]

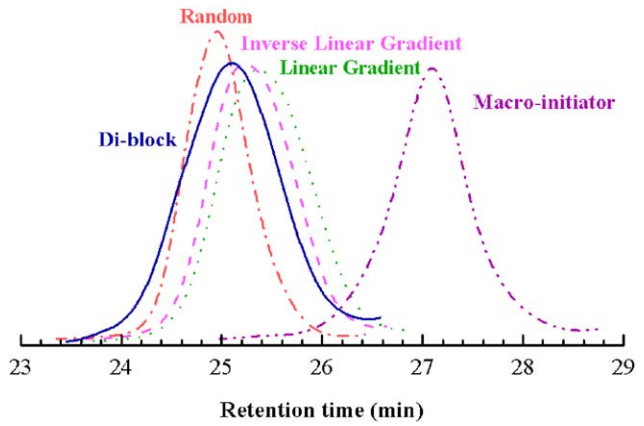

Figure 4. GPC traces of the synthesis of HFBMA/HEMA-TMS copolymers and PHEMA-TMS-Br macroinitiator.

[Color figure can be viewed in the online issue, which is available at wileyonlinelibrary.com]

Table 2. Summary of Experimental Results for the Studied System

Copolymer	M_n (Calc.) (g/mol)[a]	M_n (GPC) (g/mol)[a]	PDI (GPC)[a]	M_n (Calc.) (g/mol)[b]	DPn_{HEMA}	F_{HEMA}
Linear gradient	15,200	17,100	1.20	14,260	13	0.21
Diblock[c]	15,910	18,200	1.25	12,160	52	0.72
Random	15,960	18,500	1.16	12,420	49	0.69
Inverse linear gradient	15,700	17,500	1.19	12,310	47	0.67

[a]HFBMA/HEMA-TMS system.
[b]HFBMA/HEMA system.
[c]Prepared from PHEMA-TMS-Br (M_n(GPC) = 7970 g/mol, PDI = 1.15).

composition (F_{inst}) of the copolymer chains is not experimentally measurable. F_{cum} was measured using ^{1}H NMR, and F_{inst} was in turn calculated from the following equation: $F_{inst} = [Conv._{total,i} \times F_{cum,M2,i} - Conv._{total,i-1} \times F_{cum,M2,i-1}]/[Conv._{total,i} - Conv._{total,i-1}]$, where $Conv._{total}$ is the total conversion of both monomers (HFBMA and HEMA-TMS).[61–63] It should be noted that the F_{inst} curves for feeding monomer as a function of the degree of polymerization (Figure 3) virtually show true gradient profiles along a chain in contrast to F_{cum}. Furthermore, the cumulative compositions of random and block copolymers during the reaction period are in a good agreement with the modeling results.

From Figure 3, the instantaneous composition of feeding monomer increases continuously with the increase of the average polymer chain. For gradient copolymerization, the instantaneous compositions of both feeding monomers (HEMA-TMS and HFBMA) increase from 0 at the beginning of polymerization to about 0.83 (mole faction) at the end of both synthetic routes. The linear relationships between the instantaneous composition and degree of polymerization show clearly that the ideal gradient composition was formed gradually. This result demonstrates that the model-based semibatch process yields HFBMA/HEMA-TMS-gradient copolymers. Moreover, the variation of instantaneous composition of feeding monomer via the two modes is slightly different in total chain length and linearity. These results confirm that the introduction of particular gradient patterns in the macromolecular chains is achieved and the composition in the chain structure changes differently with the addition mode.

The GPC measurement has been used to determinate molecular weight (M_n) and molecular weight distribution (M_w/M_n, PDI) of the macroinitiator and the resulting copolymers. Figure 4 shows GPC traces of the resulting polymers. The elution peaks are symmetric and exhibit no tailing at the lower-molecular-weight-side. The narrow molecular weight distribution of the resulting copolymers suggests that the reaction proceeded in a controlled manner. The M_n data of HFBMA/HEMA copolymers were calculated. All the results are listed in Table 2.

Thermal properties of the resulting copolymers

The four fluorinated copolymers with different chain structures were characterized with DSC to compare their glass transition behaviors. Figure 5 provides the DSC heating curves of the HFBMA/HEMA copolymers with different F_{HEMA} values. It indicates that the random copolymer (Expt.3, $F_{HEMA} = 0.69$) possesses a single, narrow T_g region (ΔT_g) while the block copolymer (Expt.4, $F_{HEMA} = 0.72$) possesses two discernable T_g regions. The ΔT_g of random copolymer is about 10°C (from 35 to 45°C), similar to the glass transition behavior of homopolymers. Such a narrow transition range indicates a lack of nanoscopic heterogeneity, at least within the sensibility range of DSC. The block copolymer exhibits two T_gs in Figure 5. The first one, T_{g1}, from 30 to 40°C is associated with the HFBMA-rich domains and is lower than the value of PHFBMA (≈50°C for DPn = 20, Supporting Information, Figure S1) determinated in our study; the second, performed at higher temperature with some narrow ΔT_g (from 50 to 60°C), is associated with HEMA-rich domains and is consistent with the classic T_g response of PHEMA (≈55°C for DPn = 52, Supporting Information, Figure S1). This result indicates microphase separation with probably cylinderical morphology. The reason why the T_g responses of random and block copolymers are lower than the two homopolymers is ambiguous but it is likely due to the interacting effect of the hydroxyl group in HEMA and the tendency of stronger phase separation of the two comonormers.[64]

In contrast, the linear gradient copolymer (Expt.1, $F_{HEMA} = 0.21$) and inverse linear gradient copolymer (Expt.2, $F_{HEMA} = 0.67$) exhibit one relatively broad T_g region, which is at about 20°C (from 30 to 50°C) and 30°C (from 30 to 60°C), respectively. The T_g breadths of the linear and inverse linear gradient copolymers are greater than those of the random copolymer and of each block component in the block copolymer. These broad T_g responses can be attributed to the linear gradient composition profiles expected for nanophase-segregated gradient copolymers.[65,66] However, due to the minor difference of these two pure homopolymers' T_g responses ($T_{gPHEMA} \approx 55$°C, $T_{gPHFBMA} \approx 50$°C), the glass transition regions of two gradient copolymers do not largely expand. Furthermore, the difference of glass

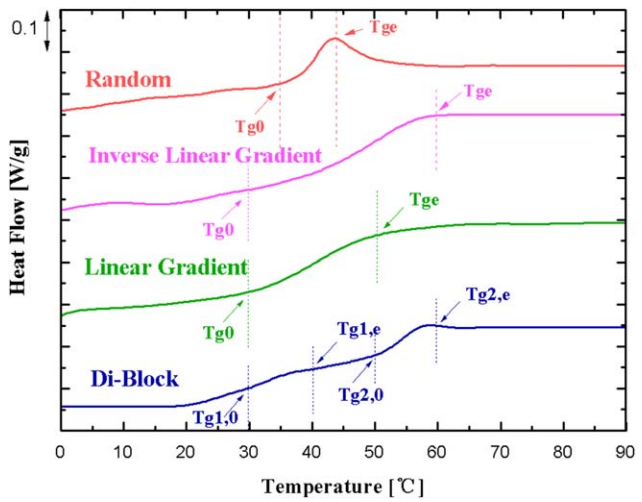

Figure 5. DSC heating curves for the HFBMA/HEMA copolymers.

[Color figure can be viewed in the online issue, which is available at wileyonlinelibrary.com]

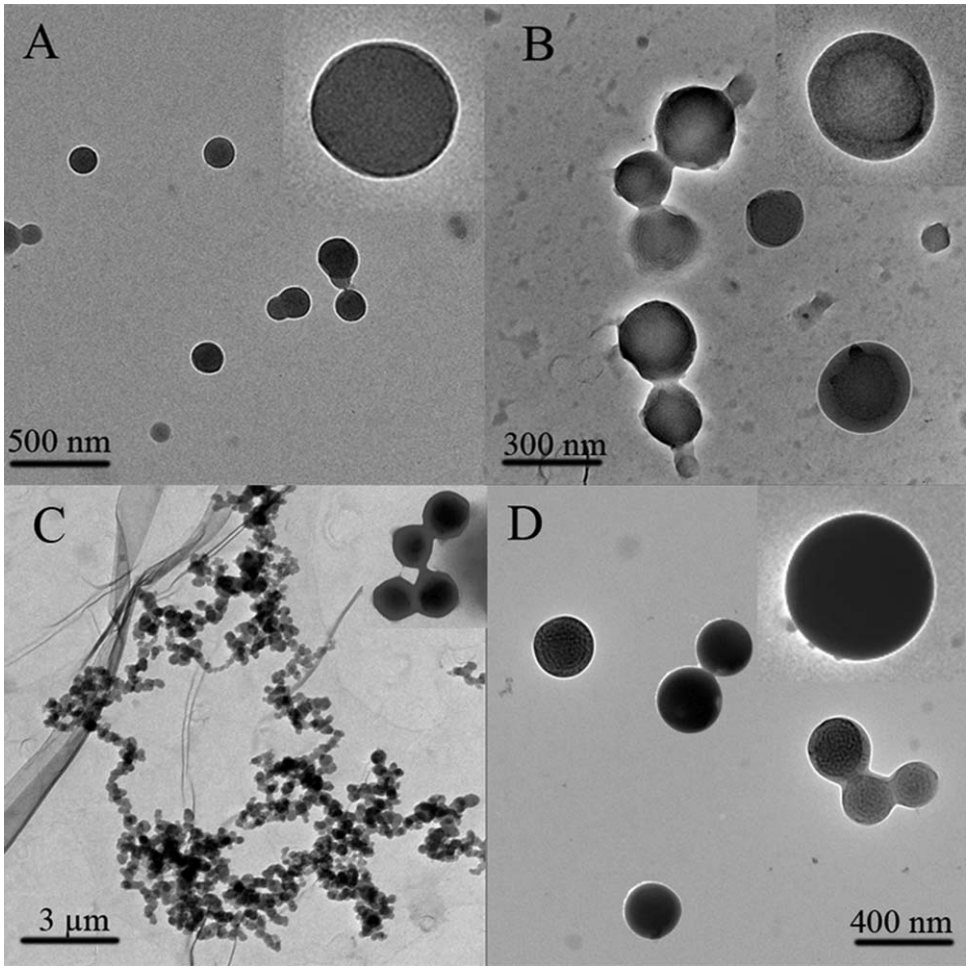

Figure 6. TEM images of the self-assembling patterns of HFBMA/HEMA copolymers (A. linear gradient copolymer; B. block copolymer; C. random copolymer; D. inverse linear gradient copolymer).

transition regions (20 and 30°C) between linear and inverse linear gradient copolymers maybe results from the different copolymer composition. Specifically, the M_ns of them are similar to each other based on two reaction modes (linear gradient, $M_n = 15{,}200$ g/mol; inverse linear gradient, $M_n = 15{,}700$ g/mol), but the HEMA content of linear gradient copolymer ($F_{HEMA} = 0.21$) is substantially lower than that of inverse gradient copolymer ($F_{HEMA} = 0.67$), which means the higher T_g attributed to PHEMA should considerably weaken. Thus, in accordance with theory,[65,66] both macromolecular chain structures and gradient profile are effective in controlling the level of nanophase separation and thermal properties of the copolymers.

Self-assembly behaviors of resulting copolymers in dilute solvent

These synthesized copolymers having amphiphilic structures, which are expected to form organized micelle structures in aqueous solution. Generally, micelles can be formed in an aqueous environment by dissolution of the copolymer in an organic solvent and then followed by dialysis against water or followed by the addition of water dropwise to the solution using mild stirring. Obviously, the latter method is simple and practicable.[67] In this work, the amphiphilic P(HEMA-HFBMA) random, block, and gradient copolymers were dissolved in THF as an appropriate nonselective solvent and the micellization was then triggered simply by adding water into the copolymer/THF solution. The micellar behaviors were monitored by TEM and DLS.

As shown in Figure 6, all the synthesized copolymers are prone to form spherical micelles. They display a relatively uniform size distribution, with an average diameter of ~200–220 nm (A), 250–280 nm (B), 300–400 nm (C), and 200–250 nm (D). In addition, one knows that the aggregate formation in solution depends on many factors including composition, sequence, relative lengths of the hydrophobic and hydrophilic segments, and so forth.[68] Obvious differences indeed exist between these four TEM images. First, the neat spherical morphology is formed by the self-assembly of linear (A) and inverse linear (D) gradient copolymers in dilute solution; second, the micelles of block copolymer (B) seem to have some deformity, but with apparent core-corona structure; thirdly, most micelles of random copolymer (C) have a spherical shape but aggregate to some extent, which often consist of dense hydrophobic cores surrounded by a corona of swollen loops formed by the hydrophilic parts of the polymer.

DLS has been used to detect the sizes of aggregates in solution. Different from TEM, an average-size and size distribution were recorded for each solution directly by DLS (Figure 7). From Figure 7, the results reveal that the size

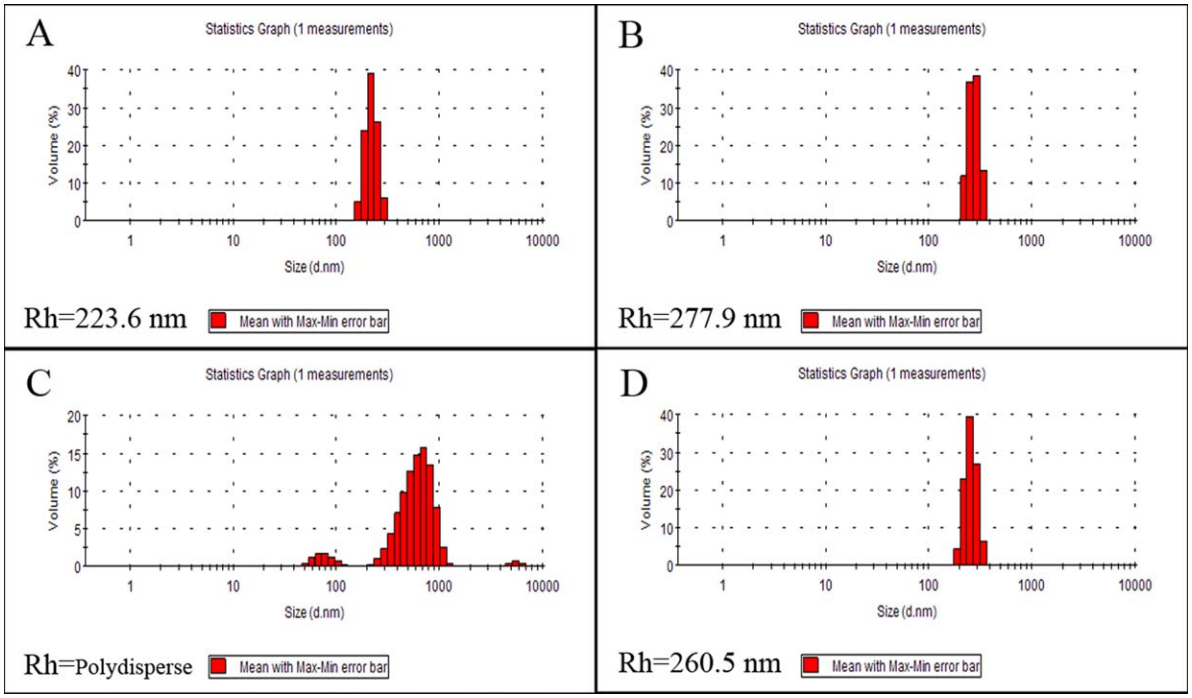

Figure 7. DLS results of the micellar solution HFBMA/HEMA copolymers (A. linear gradient copolymer; B. block copolymer; C. random copolymer; D. inverse linear gradient copolymer).

[Color figure can be viewed in the online issue, which is available at wileyonlinelibrary.com]

distribution is relatively uniform, with an average diameter of ~223.6 nm (A), 277.9 nm (B), and 260.5 nm (D). However, the size distribution of random copolymers is more polydispersed, which is attributed to their aggregation to a certain extent. Due to different measurement conditions, the diameters obtained from DLS are slightly larger than those determined by TEM.

Theoretically, morphology is mainly controlled by a force balance involving stretching of the core chains, surface tension between the core and the outside solvent, and repulsion among the corona polymer chains.[69] In essence, the formation of micelles is a requirement for a micellar system to minimize its free energy. As for the gradient copolymers, a small fraction of the HEMA and HFBMA units consisting of a gradient chain microstructure should be embedded in the core domains, which results in a relatively weak-phase separation. This provides a tentative explanation for the fuzzy core-corona transition of the aggregates. In contrast to the gradient copolymers, the copolymer having two incompatible blocks provokes an aggregation of PHFBMA blocks into dense hydrophobic domain surrounded by a protective corona of soluble blocks. In dilute solutions, this association leads to the formation of nanoscale discrete aggregates. However, the formation of the spherical structure from the random copolymer can be attributed to the fact that the solvent becomes progressively less favorable for the hydrophobic segments of the P(HEMA-ran-HFBMA). Some HEMA units probably segregate to the interface (small hydrophilic loops) between the aggregates and the external aqueous solution, which serve to stabilize the aggregates. When the water content is low, the interiors of the aggregates have a relatively low viscosity (loose chain distribution without gathering into a dense core), and the exterior of the spheres is soft. The low viscosity leads to a rapid solvent diffusion in and out of the soft loop and a homogeneous shrinkage of the whole aggregate.[70] Namely, the formation of the loops leads to smaller hydrophilic corona as well as less defined and less stable aggregates. To achieve a more stable state, the dispersive micelles are inclined to aggregate together to form the large-compound micelles. On the other hand, a certain number of fluorinated side chains in the hydrophilic loop can be expected, because a complete separation of hydrophilic and hydrophobic parts will be precluded by steric hindrance and unfavorable entropy term.[71]

Based on the above TEM and DLS analysis for morphologies and sizes of micelles, as well as theoretical interpretation, the proposed structures for spherical micelles in THF/H_2O are illustrated schematically in Scheme 3.

Surface properties of the resulting copolymers membranes

Generally speaking, a flat polymer membrane surface with low energy exhibits SWCA values in the range of 100–120°.[48,49] The contact angle is defined as the angle between the substrate surface and the tangential line at the point of contact of the liquid droplet with the substrate. A higher contact angle means that the surface of the membrane has become more hydrophobic. Figure 8 and Table 3 descript the results of SWCA measurements and the calculated surface free energies (γ_s) of HEMA/HFBMA copolymers membranes. The SWCA and γ_s of diblock, random, and inverse linear gradient copolymers with similar fluorine content ($W_F = 22.12$, 23.57, 25.01%) are 109, 108, 116°, and 17.62, 18.20, 13.67 mN/m, respectively. We speculate that the hydrophobic surface with a SWCA lower than 120° is attributed to two opposite effects. On one hand, the solubility of PHEMA in a poor polar solvent (here THF) decreases when the DP_n becomes larger, therefore, the solvophilic component (HFBMA) collects onto the membrane surface for the

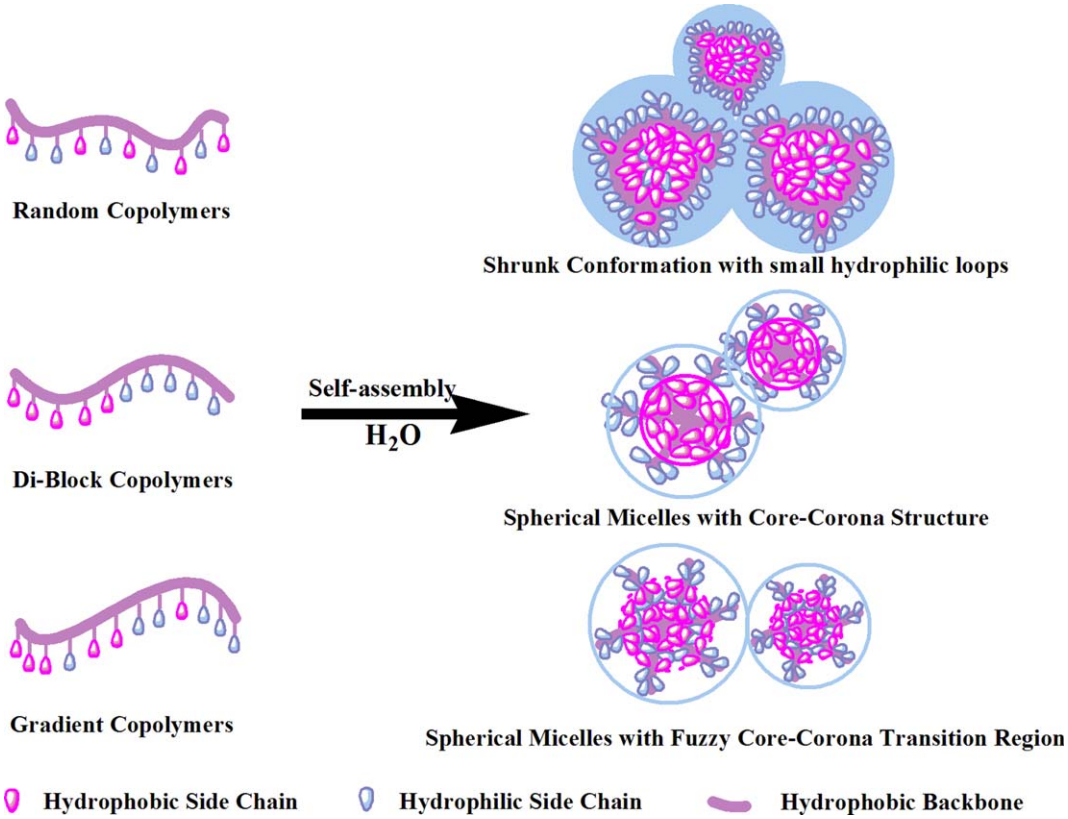

Scheme 3. Schematic illustrations of spherical micelles in THF/H_2O (Top) aggregate with random structure; (Middle) aggregate with core-corona structure; (Bottom) aggregate with fuzzy core-corona structure.

[Color figure can be viewed in the online issue, which is available at wileyonlinelibrary.com]

generation of lowγ_s. This makes the polymer solution prone to self-assemble into aggregates. On the other hand, it is inevitable that a part of the hydrophilic components emerges on the surface result in lowering the contact angle. However, the linear gradient copolymer with the highest fluorine content ($W_F = 43.84$ %) exhibits the largest SWCA (131°) and lowest γ_s (6.43 mN/m) as expected. The surface characterization convincingly demonstrates that the synthetic copolymers of the fluoromonomer are also a low-surface energy material.

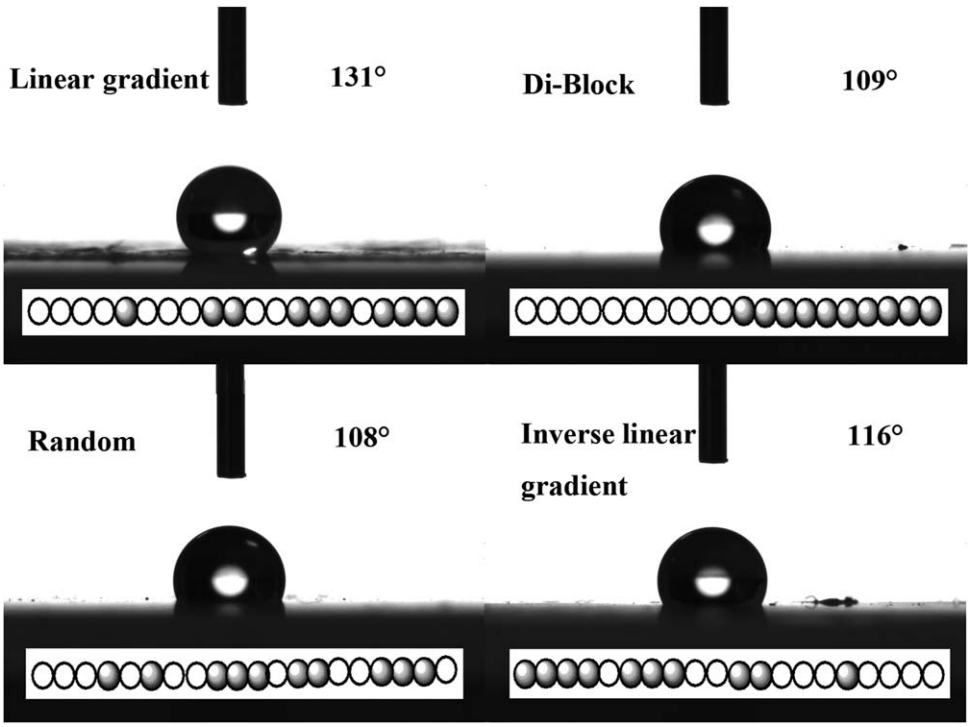

Figure 8. Static water contact angels of the HFBMA/HEMA copolymers.

Table 3. Surface Properties and XPS Quantification of HEMA/HFBMA Copolymers Membranes

Copolymer	W_F[a] (%) (in Bulk)	θ_{H2O} (°)	γ_s[b] (mN/m)	C 1s (%)	O 1s (%)	F 1s (%)
Linear gradient	43.84	131°	6.43	41.68	15.23	43.09
Di-Block	22.12	109°	17.62	53.79	19.50	26.71
Random	23.57	108°	18.20	56.66	20.27	23.07
Inverse linear gradient	25.01	116°	13.67	50.75	18.90	30.35

[a]W_F is the weight percent of fluorine obtained from the equations: $F\% = (7*19*DP_n)/(M_n(\text{Calc.}))$, where each fluorinated monomer HFBMA contains seven fluorine atoms and the fluorine atomic weight is 19 and DPn is polymerization degree of the PHFBMA.
[b]Calculated from a new equation: $1+\cos\theta = 2(\gamma_S/\gamma_L)^{1/2}\exp[-\beta(\gamma_L-\gamma_S)^2]$ derived by Li and Neumann,[72] where γ_S, γ_L, and θ represents the surface energy of polymer, water, and the static water angel, respectively.

Additionally, to further understand the reason leading to the differences of surfaces properties in these four copolymers, XPS was applied to study the surface compositions of the polymer membranes. Figure 9 is a broad scan of the binding energy spectrum from 0 to 960 eV for four copolymer membranes. The XPS images of the four samples obtained are alike with each other and strong characteristic signals of carbon, oxygen, and fluorine are found as expected. From Figure 9, the surface survey scan of XPS shows four strong and one weak peak, at ~835, 687, 532, 285, and 32 eV, which result from direct photoionization from F KLL, F 1s, O 1s, C 1s, and F 2s core levels, respectively. The atomic contents of C 1s, O 1s, and F 1s calculated by software are listed in Table 3. We found that the topmost surfaces of diblock and inverse linear gradient polymer membranes were enriched in fluorine with respect to the bulk. Many other examples have been reported in the literature about the selective segregation of semifluorinated chains of a polymeric structure at the polymer-air interface, because of their low-surface energy.[73–76] This phenomenon might be improved owing to the tendency of self-assembly of hydrocarbon segments with alkyl groups. Nevertheless, the results for linear gradient and random copolymers are nearly the same. The linear gradient copolymer having the same fluorine content consists of a majority of HFBMA ($F_{HFBMA} = 0.79$) and a minority of HEMA, which results in good solubility in THF; whereas the advantage of the random copolymer is its excellent component compatibility, namely, it is uniform at the nanoscale. Therefore, their surface properties might result from the semifluorinated segments of the side chains appeared to be stretched out at the polymer-air interface, with the terminal CF_3 groups pointing outward.

The polymer solutions were examined by TEM, Figure 10 reveals that the linear gradient (A) and random (C) copolymers, which dissolved well in THF, do not aggregate and just appear mutual entanglement of macromolecular chains. Surprisingly, the TEM images show both diblock (B) and inverse gradient copolymers (D) aggregate into spherical-like morphology with fuzzy core and vivid but discrete corona. It

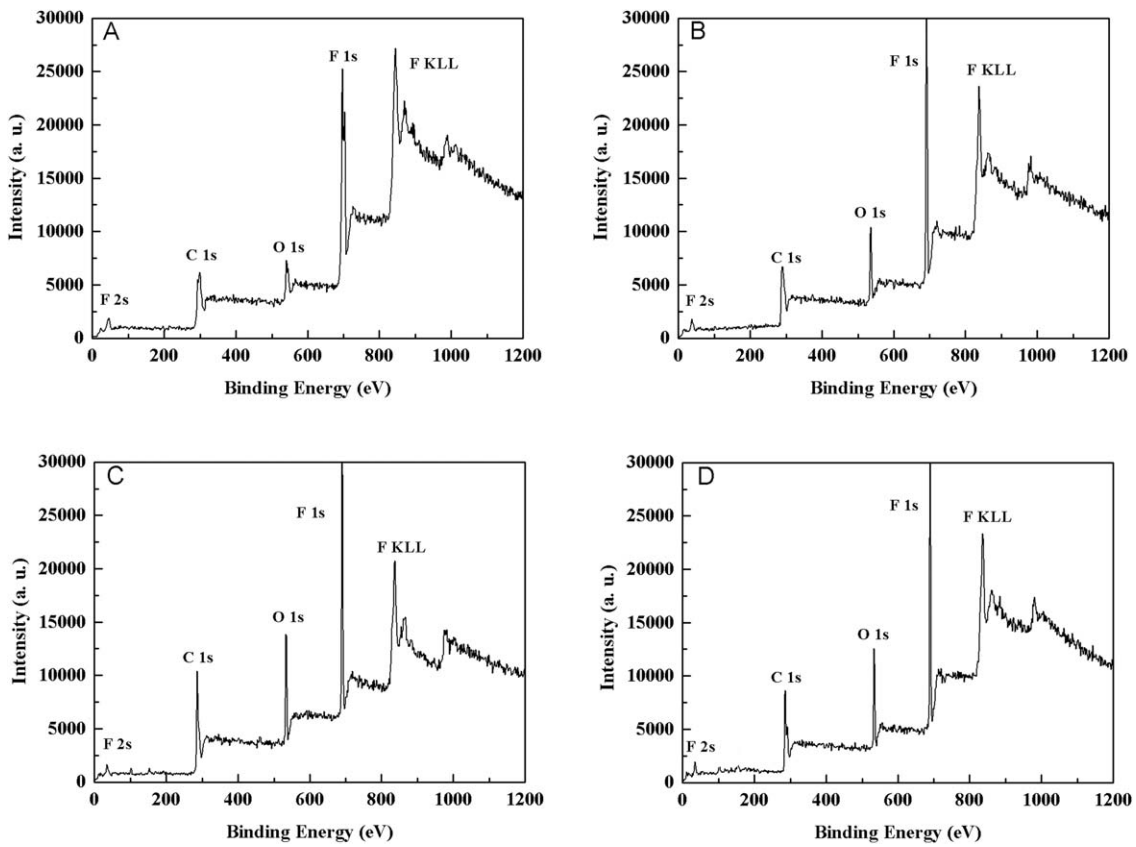

Figure 9. XPS scanning spectra for air-side surfaces of the HFBMA/HEMA copolymers (A. linear gradient copolymer; B. block copolymer; C. random copolymer; D. inverse linear gradient copolymer).

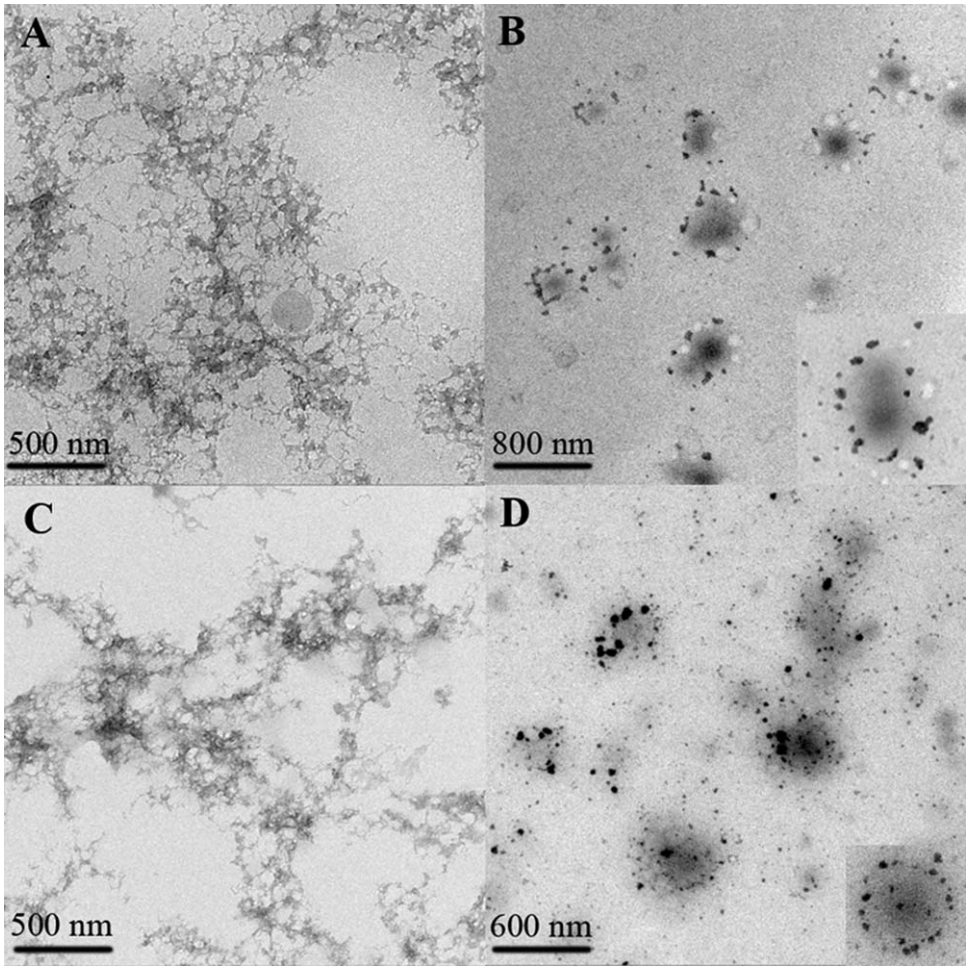

Figure 10. TEM images of morphology of HFBMA/HEMA copolymers in THF (A. linear gradient copolymer; B. block copolymer; C. random copolymer; D. inverse linear gradient copolymer).

should be pointed out that the aggregation presented here significantly differs from those nanoassembly discussed above. The scattered black spots might be identified as clustered macromolecular chains. But the driving force for these spots gathering into annular structures is still vague. This intriguing finding drives us to further in-depth research on it. Nevertheless, the extraordinary result partly confirms what we have speculated previously.

Based on the above information, the proposed aggregation behavior model of macromolecular chains on the surfaces of a copolymer membrane with different structures (random and linear gradient copolymers belong to Mode A, named Normal Mode; diblock and inverse linear gradient copolymers pertain to Mode B, named "Self-Assembly" Mode) is shown in Scheme 4.

Conclusions

In this work, a combinatory approach coupling theoretical modeling and an experimental study was presented for

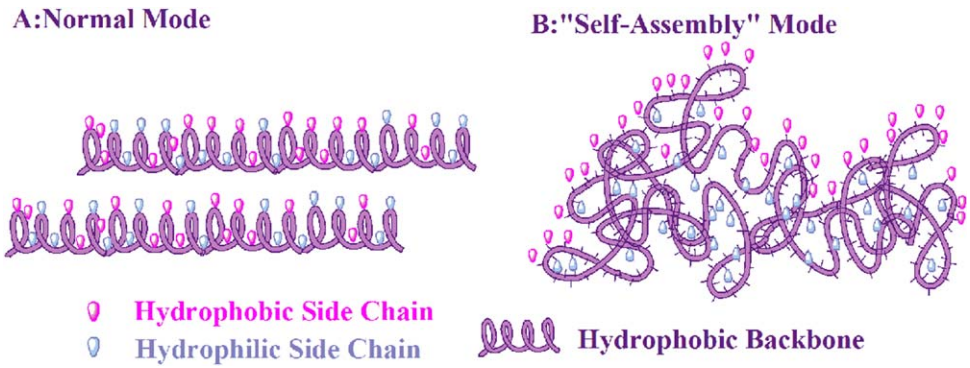

Scheme 4. The proposed aggregation behavior model of macromolecular chains on the surfaces of copolymer membrane with different structures (A: Nature Mode; B: "Self-Assembly" Mode).

[Color figure can be viewed in the online issue, which is available at wileyonlinelibrary.com]

optimization, preparation, and characteristic comparison of the amphiphilic copolymers of HFBMA and HEMA to achieve a multiscale generalization of this polymer system. This study clearly demonstrates the effect of synthesis methodology on the molecular structure. Base on theory models, batch copolymerization leads exclusively to random copolymer, and diblock copolymer can be produced by sequential homopolymerization. Meanwhile, semibatch polymerization based on the developed model can easily be performed to create polymeric materials having a gradient composition. Furthermore, this research has investigated the remarkable properties of fluorinated copolymers of different CCD.

First, different thermal properties of copolymers resulting from the various compositional heterogeneities are controlled by the CCD. The random copolymer possesses a single, narrow T_g region (ΔT_g) and the block copolymer possesses two discernable T_g regions. In contrast, the linear gradient and inverse linear gradient copolymers exhibit one broad T_g region but a significantly different breadth.

Second, the aggregation of these four copolymers in THF/H_2O solution was investigated by TEM and DLS, and the results show that their morphology and size depend strongly on CCD. TEM images show that the aggregates have an average diameter of ~200–220 nm (A), 250–280 nm (B), 300–400 nm (C), and 200–250 nm (D) for different copolymers, respectively, which are also confirmed by DLS;

Thirdly, the surface properties were determined by SWCA and XPS. The behavior of copolymer in solution is revealed by TEM. The surface characterizations demonstrate that the copolymers of fluoromonomer have low-surface energy. Particularly, the linear gradient copolymer has SWCA as high as 131°. Furthermore, the TEM results demonstrate that diblock and inverse linear gradient copolymers have a tendency to form lager micelles in THF, yielding different fluorine content in bulk and at the surface. But this discrepancy is not found in linear gradient and random copolymer membranes due to the composition and component compatibility. Further research is in progress. Remarkably, controlling the CCD can, thus, give rise to distinctively different macroscopic surface property of materials.

In summary, theoretical modeling can be used to optimize the macromolecular structures for tuning the properties of polymeric materials. However, our current work is only preliminary because a multiscale generalization of polymeric system from design to practical application is very complicated and difficult. Further studies on the multiscale generalization of polymeric systems are ongoing.

Acknowledgments

The authors thank the National Ministry of Science and Technology of China (No. 2012CB21500402), the National Natural Science Foundation of China (No. 21076171, 21276213), and the State-Key Laboratory of Chemical Engineering of Tsinghua University (No. SKL-ChE-10A03) for supporting this work. The authors would like to thank Dr. Zhibin Ye (Laurentian University, Canada), Professor Garry Rempel (University of Waterloo, Canada), and Professor Qinmin Pan (Soochow University) for their kind suggestions and meaningful contribution to the manuscript.

Literature Cited

1. Reisinger JJ, Hillmyer MA. Synthesis of fluorinated polymers by chemical modification. *Prog Polym Sci*. 2002;27:971–1005.
2. Hansen NML, Jankova K, Hvilsted S. Fluoropolymer materials and architectures prepared by controlled radical polymerizations. *Eur Polym J*. 2007;43:255–293.
3. Yamaguchi H, Kikuchi M, Kobayashi M, Ogawa H, Masunaga H, Sakata O, Takahara A. Influence of molecular weight dispersity of poly{2-(perfluorooctyl)ethyl acrylate} brushes on their molecular aggregation states and wetting behavior. *Macromolecules*. 2012;45:1509–1516.
4. Hillmyer MA, Lodge TP. Synthesis and self-assembly of fluorinated block copolymers. *J Polym Sci Part A: Polym Chem*. 2002;40:1–8.
5. Mielczarski JA, Mielczarski E, Galli G, Morelli A, Martinelli E, Chiellini E. The surface-segregated nanostructure of fluorinated copolymer-poly(dimethylsiloxane) blend films. *Langmuir*. 2010;26:2871–2876.
6. Sundaram HS, Cho Y, Dimitriou MD, Finlay JA, Cone G, Williams S, Handlin D, Gatto J, Callow ME, Callow JA, Kramer EJ, Ober CK. Fluorinated amphiphilic polymers and their blends for fouling-release applications: the benefits of a triblock copolymer surface. *ACS Appl Mater Interfaces* 2011;3:3366–3374.
7. Yi L, Huang C, Zhou W. Synthesis, surface properties, and morphologies of poly[methyl(3,3,3-trifluoropropyl)siloxane]-*b*-polystyrene-*b*-poly(*tert*-butyl acrylate) triblock copolymers by a combination of anionic ROP and ATRP. *J Polym Sci Part A: Polym Chem*. 2012;50:1728–1739.
8. Sawada H, Tashima T, Nishiyama Y, Kikuchi M, Goto Y, Kostov G, Ameduri B. Iodine transfer terpolymerization of vinylidene fluoride, α-trifluoromethacrylic acid and hexafluoropropylene for exceptional thermostable fluoropolymers/silica nanocomposites. *Macromolecules*. 2011;44:1114–1124.
9. Uragmi T, Yamada H, Miyata T. Effects of fluorine-containing graft and block copolymer additives on removal characteristics of dilute benzene in water by microphase-separated membranes modified with these additives. *Macromolecules*. 2006;39:1890–1897.
10. Inoue Y, Watanabe J, Takai M, Yusa S, Ishihara K. Synthesis of sequence-controlled copolymers from extremely polar and apolar monomers by living radical polymerization and their phase-separated structures. *J Polym Sci Part A: Polym Chem*. 2005;43:6073–6083.
11. Seifert LM, Greer RT. Evaluation of in vivo adsorption of blood elements onto hydrogel-coated silicone rubber by scanning electron microscopy and Fourier transform infrared. *J Biomed Mater Res*. 1985;19:1043–1071.
12. Alvarez-Lorenzo C, Hiratani H, Gómez-Amoza JL, Martínez-Pacheco R, Souto C, Concheiro A. Soft contact lenses capable of sustained delivery of timolol. *J Pharm Sci*. 2002;91:2182–2192.
13. Mijajima M, Okano T, Kim SW, Higushi WI. Preformulation of an Ara-A transdermal delivery system: Membrane fabrication and characterization. *J Controlled Release*. 1987;5:179–186.
14. Montheard JP, Kahovec J, Chappard D. In: Arshady R, editor. Desk Reference of Functional Polymers Syntheses and Applications, Chapter 5.3, Washington, DC: American Chemical Society, 1997.
15. Zhang Y, Chu DF, Zheng MY, Kissel T, Agarwal S. Biocompatible and degradable poly(2-hydroxyethyl methacrylate) based polymers for biomedical applications. *Polym Chem*. 2012;3:2752–2759.
16. Weaver JVM, Bannister I, Robinson KL, Azeau XB, Armes SP, Smallridge M, McKenna P. Stimulus-responsive water-soluble polymers based on 2-hydroxyethyl methacrylate. *Macromolecules*. 2004;37:2395–2403.
17. Wolf FF, Friedemann N, Frey H. Poly(lactide)-block-poly(HEMA) block copolymers: an orthogonal one-pot combination of ROP and ATRP, using a bifunctional initiator. *Macromolecules*. 2009;42:5622–5628.
18. Johnson RP, Jeong Y-I, Choi E, Chung C-W, Kang DH, Oh S-O, Suh H, Kim I. Biocompatible poly(2-hydroxyethyl methacrylate)-*b*-poly(L-histidine) hybrid materials for pH-sensitive intracellular anticancer drug delivery. *Adv Funct Mater*. 2012;22:1058–1068.
19. Luo Y, Liu L, Wang X, Shi H, Lv W, Li J. Sugar-installed thermoresponsive micellar aggregates self-assembled from ''coil-comb-coil'' triblock glycopolymers: preparation and recognition with Concanavalin A. *Soft Matter*. 2012;8:1634–1642.
20. Oh JK, Dong H, Zhang R, Matyjaszewski K, Schlaad H. Preparation of nanoparticles of double-hydrophilic PEO-PHEMA block copolymers by AGET ATRP in inverse miniemulsion. *J Polym Sci Part A: Polym Chem*. 2007;45:4764–4772.
21. Zhao X, Liu W, Chen D, Lin X, Lu WW. Effect of block order of ABA- and BAB-type NIPAAm/HEMA triblock copolymers on thermoresponsive behavior of solutions. *Macromol Chem Phys*. 2007;208:1773–1781.

22. Qin S, Saget J, Pyun J, Jia S, Kowalewski T, Matyjaszewski K. Synthesis of block, statistical and gradient copolymers from octadecyl (meth)acrylates using atom transfer radical polymerization. *Macromolecules*. 2003;36:8969–8977.
23. Matyjaszewski K. Ziegler MJ, Arehart SV, Greszta D, Pakula T. Gradient copolymers by atom transfer radical copolymerization. *J Phys Org Chem*. 2000;13:775–786.
24. Lefebvre MD, Dettmer CM, McSwain RL, Xu C, Davila JR., Composto RJ, Nguyen ST, Shull KR. Effect of sequence distribution on copolymer interfacial activity. *Macromolecules*. 2005;38:10494–10502.
25. Kim J, Mok MM, Sandoval RW, Woo DJ, Torkelson JM. Uniquely broad glass transition temperatures of gradient copolymers relation to random and block copolymers containing repulsive comonomers. *Macromolecules*. 2006;39:6152–6160.
26. Wong CLH, Kim J, Torkelson JM. Breadth of glass transition temperature in styrene/acrylic acid block, random, and gradient copolymers: unusual sequence distribution effects. *J Polym Sci Part B: Polym Phys*. 2007;45:2842–2849.
27. Mok MM, Kim J, Torkelson JM. Gradient copolymers with broad glass transition temperature regions: design of purely interphase compositions for damping applications. *J Polym Sci Part B: Polym Phys*. 2008;46:48–58.
28. Sun XY, Luo YW, Wang R, Li BG, Zhu SP. Semibatch RAFT polymerization for producing ST/BA copolymers with controlled gradient composition profiles. *AIChE J*. 2008;54:1073–1087.
29. Mok MM, Ellison CJ, Torkelson JM. Effect of gradient sequencing on copolymer order–disorder transitions: phase behavior of styrene/*n*-butyl acrylate block and gradient copolymers. *Macromolecules*. 2011;44:6220–6226.
30. Zhou YN, Li JJ, Luo ZH. Synthesis of gradient copolymers with simultaneously tailor-made chain composition distribution and glass transition temperature by semibatch ATRP: from modeling to application. *J Polym Sci Part A: Polym Chem*. 2012;50:3052–3066.
31. Bruno A. Controlled Radical (co)polymerization of fluoromonomers. *Macromolecules*. 2010;43:10163–10184.
32. Hawker CJ, Bosman AW, Harth E. New polymer synthesis by nitroxide mediated living radical polymerization. *Chem Rev*. 2001;101:3661–3688.
33. Lacroix-Desmazes P, Andre P, Desimone JM, Ruzette AV, Boutevin B. Macromolecular surfactants for supercritical carbon dioxide applications: synthesis and characterization of fluorinated block copolymers prepared by nitroxide-mediated radical polymerization. *J Polym Sci Part A: Polym Chem*. 2004;42:3537–3552.
34. Matyjaszewski K, Xia JH. Atom transfer radical polymerization. *Chem Rev*. 2001;101:2921–2990.
35. Kamigaito M, Ando T, Sawamto M. Metal-catalyzed living radical polymerization. *Chem Rev*. 2001;101:3689–3746.
36. Borkar S, Sen A. Novel fluoroalkene-methyl acrylate copolymers by atom transfer radical polymerization. *Macromolecules*. 2005;38:3029–3032.
37. Luo ZH, He TY. Synthesis and characterization of poly(dimethylsiloxane)-block-poly (2,2,3,3,4,4,4-heptafluorobutyl methacrylate) diblock copolymers with low surface energy prepared by atom transfer radical polymerization. *React Funct Polym*. 2008;68:931–942.
38. Chiefari J, Chong YK, Ercole F, Krstina J, Jeffrey J, Le TPT, Mayadunne RTA, Meijs GF, Moad CL, Moad G, Rizzardo E, Thang SH. Living free-radical polymerization by reversible addition-fragmentation chain transfer: the RAFT process. *Macromolecules*. 1998;31:5559–5562.
39. Girard E, Marty J-D, Ameduri B, Destarac M. Direct synthesis of vinylidene fluoride-based amphiphilic diblock copolymers by RAFT/MADIX polymerization. *ACS Macro Lett*. 2012;1:270–274.
40. Rosen BM, Percec V. Single-electron transfer and single-electron transfer degenerative chain transfer living radical polymerization. *Chem Rev*. 2009;109:5069–5119.
41. Wilson CJ, Wilson DA, Feiring AE, Percec V. Disassembly via an environmentally friendly and efficient fluorous phase constructed with dendritic architectures. *J Polym Sci Part A: Polym Chem*. 2010;48:2498–2508.
42. Wang L, Broadbelt LJ. Explicit sequence of styrene/Methyl Methacrylate gradient copolymers synthesized by forced gradient copolymerization with nitroxide-mediated controlled radical polymerization. *Macromolecules*. 2009;42:7961–7968.
43. Wang L, Broadbelt LJ. Model-Based design for preparing styrene/methyl methacrylate structural gradient copolymers. *Macromol Theory Simul*. 2011;20:191–204.
44. Wang R, Luo Y, Li B, Sun X, Zhu S. Design and control of copolymer composition distribution in living radical polymerization using semibatch feeding policies: a model simulation. *Macromol Theory Simul*. 2006;15:356–368.
45. Wang R, Luo YW, Li BG, Zhu SP. Control of gradient copolymer composition in ATRP using semibatch feeding policy. *AIChE J*. 2007;53:174–186.
46. Sun XY, Luo YW, Wang R, Li BG, Liu B, Zhu SP. Programmed synthesis of copolymer with controlled chain composition distribution via semibatch RAFT copolymerization. *Macromolecules*. 2007;40: 849–859.
47. Zhao Y, Luo YW, Ye CH, Li BG, Zhu SP. Model-based design and synthesis of gradient MMA/tBMA copolymers by computer-programmed semibatch atom transfer radical copolymerization. *J Polym Sci Part A: Polym Chem*. 2009;47:69–79.
48. Luo ZH, He TY, Yu HJ, Dai LZ. Novel ABC triblock copolymer with very low surface energy: Poly(dimethylsiloxane)-*block*-Poly(-methyl methacrylate)-*block*- Poly(2,2,3,3,4,4,4-heptafluorobutyl methacrylate). *Macromol React Eng*. 2008;2:398–406.
49. Yu HJ, Luo ZH. Novel superhydrophobic silica/poly(siloxane-fluoroacrylate) hybrid nanoparticles prepared via two-step surface-initiated ATRP: synthesis, characterization, and wettability. *J Polym Sci Part A: Polym Chem*. 2010;48:5570–5580.
50. Liang J, He L, Zhao X, Dong X, Luo H, Li W. Novel linear fluorosilicon-containing pentablock copolymers: synthesis and their properties as coating materials. *J Mater Chem*. 2011;21:6934–6943.
51. Tan BH, Hussain H, Liu Y, He CB, Davis TP. Synthesis and self-assembly of brush-type poly [poly (ethylene glycol) methyl ether methacrylate]-block-poly (pentafluorostyrene) amphiphilic diblock copolymers in aqueous solution. *Langmuir*. 2010;26:2361–2368.
52. Qiu JJ, Luo ZH. Self-assembly of ABC nonamphiphilic fluorosilicone triblock copolymers in dilute solutions: the first example. *J Polym Sci Part A: Polym Chem*. 2011;49:2513–2519.
53. Cheng H, Li JJ, Luo ZH. Regular polygonal micelles induced from fluorosilicone diblock copolymers. *J Polym Sci Part A: Polym Chem*. 2012;50:1249–1253.
54. Urushihara Y, Nishino T. Effects of film-forming conditions on surface properties and structures of diblock copolymer with perfluoroalkyl side chains. *Langmuir*. 2005;21:2614–2618.
55. Li Y, Meli L, Lim KT, Johnston KP, Green PF. Structural inversion of micellar block copolymer thin films. *Macromolecules*. 2006;39:7044–7054.
56. Mayo FR, Lewis FM. Copolymerization. I. A basis for comparing the behavior of monomers in copolymerization, the copolymerization of styrene and methyl methacrylate. *J Am Chem Soc*. 1944;66:1594–1601.
57. Skeist I. Copolymerization: the composition distribution curve. *J Am Chem Soc*. 1946;68:1781–1784.
58. Meyer VE, Lowry GG. Integral and differential binary copolymerization equations. *J Polym Sci A Gen Pap*. 1965;3:2843–2851.
59. Harrisson S, Ercole F, Muir BW. Living spontaneous gradient copolymers of acrylic acid and styrene: one-pot synthesis of pH-responsive amphiphiles. *Polym Chem*. 2010;1:326–332.
60. Beers KL, Boo S, Gaynor SG, Matyjaszewski K. Atom transfer radical polymerization of 2-hydroxyethyl methacrylate. *Macromolecules*. 1999;32:5772–5776.
61. Min K, Kwon Oh J, Matyjaszewski K. Preparation of gradient copolymers via ATRP in miniemulsion. II. forced gradient. *J Polym Sci Part A: Polym Chem*. 2007;45:1413–1423.
62. Zhao Y, Luo YW, Li BG, Zhu SP. pH responsivity and micelle formation of gradient copolymers of methacrylic acid and methyl methacrylate in aqueous solution. *Langmuir*. 2011;27:11306–11315.
63. Nakatani K, Ogura Y, Koda Y, Terashima T, Sawamoto M. Sequence-regulated copolymers via tandem catalysis of living radical polymerization and in situ transesterification. *J Am Chem Soc*. 2012;134:4373–4383.
64. Mok MM, Kim J, Wong CLH, Marrou SR, Woo DJ, Dettmer CM, Nguyen ST, Ellison CJ, Shull KR, Torkelson JM. Glass transition breadths and composition profiles of weaky, moderately, and strongly segregating gradient copolymers: experimental results and calculations from self-consistent mean-field theory. *Macromolecules*. 2009;42:7863–7876.
65. Lefebvre MD, de la Cruz MO, Shull KR. Phase segregation in gradient copolymer melts. *Macromolecules*. 2004;37:1118–1123.
66. Jiang R, Jin QH, Li BH, Ding DT, Wickham RA, Shi AC. Phase behavior of gradient copolymers. *Macromolecules*. 2008;41:5457–5465.

67. Tian Z, Liu X, Chen C, Allcock HR. Synthesis and micellar behavior of novel amphiphilic poly[bis(trifluoroethoxy)phosphazene]-co-poly[(dimethylamino)ethyl methacrylate] block copolymers. *Macromolecules*. 2012;45:2502–2508.
68. He YY, Li ZB, Simone P, Lodge TP. Self-assembly of block copolymer micelles in an ionic liquid. *J Am Chem Soc*. 2006;128:2745–2750.
69. Zhang L, Eisenberg A. Formation of crew-cut aggregates of various morphologies from amphiphilic block copolymers in solution. *Polym Adv Technol*. 1998;9:677–699.
70. Liu X, Kim J-S, Wu J, Eisenberg A. Bowl-shaped aggregates from the self-assembly of an amphiphilic random copolymer of poly (styrene-co-methacrylic acid). *Macromolecules*. 2005;38:6749–6751.
71. Barz M, Luxenhofer R, Zentel R, Kabanov AV. The uptake of N-(2-hydroxypropyl)-methacrylamide based homo, random and block copolymers by human multidrug resistant breast adenocarcinoma cells. *Biomaterials*. 2009;30:5682–5690.
72. Li D, Neumann AW. Contact angles on hydrophobic solid surfaces and their interpretation. *J Colloid Interface Sci*. 1992;148:190–200.
73. Tsibouklis J, Graham P, Eaton PJ, Smith JR, Nevell TG, Smart JD, Ewen RJ. Poly(perfluoroalkyl methacrylate) film structures: surface organization phenomena, surface energy determinations, and force of adhesion measurements. *Macromolecules*. 2000;33:8460–8465.
74. Martinelli E, Agostini S, Galli G, Chiellini E, Glisenti A, Pettitt ME, Callow ME, Callow JA, Graf K, Bartels FW. Nanostructured films of amphiphilic fluorinated block copolymers for fouling release application. *Langmuir*. 2008;24:13138–13147.
75. Xue, DW, Wang XP, Ni HG, Zhang W, Xue G. Surface segregation of fluorinated moieties on random copolymer films controlled by random-coil conformation of polymer chains in solution. *Langmuir*. 2009;25:2248–2257.
76. Chung J-S, Kim BG, Sohn E-H, Lee J-C. Molecular structure and surface properties of comb-like fluorinated poly(oxyethylene)s having different content of fluoroalkyl side group. *Macromolecules*. 2010;43:10481–10489.

Manuscript received Nov. 4, 2012, and revision received Feb. 1, 2013.